Article

Neural coding during active somatosensation revealed using illusory touch

O'CONNOR, Daniel H, *et al*.

nature neuroscience

Neural coding during active somatosensation revealed using illusory touch

Daniel H O'Connor[1–3], S Andrew Hires[1,3], Zengcai V Guo[1], Nuo Li[1], Jianing Yu[1], Qian-Quan Sun[1,2], Daniel Huber[1,2] & Karel Svoboda[1]

Active sensation requires the convergence of external stimuli with representations of body movements. We used mouse behavior, electrophysiology and optogenetics to dissect the temporal interactions among whisker movement, neural activity and sensation of touch. We photostimulated layer 4 activity in single barrels in a closed loop with whisking. Mimicking touch-related neural activity caused illusory perception of an object at a particular location, but scrambling the timing of the spikes over one whisking cycle (tens of milliseconds) did not abolish the illusion, indicating that knowledge of instantaneous whisker position is unnecessary for discriminating object locations. The illusions were induced only during bouts of directed whisking, when mice expected touch, and in the relevant barrel. Reducing activity biased behavior, consistent with a spike count code for object detection at a particular location. Our results show that mice integrate coding of touch with movement over timescales of a whisking bout to produce perception of active touch.

Animals explore the world by moving their sensors across objects and scenes of interest. The brain therefore must interpret sensory input in the context of sensor movement. The relative timing of neural signals representing movement (efference or reafference) and sensation (exafference) is crucial for sensorimotor integration. For example, a tickling stimulus, when self applied, does not evoke the perception of tickling; however, when the same stimulus arrives out of phase with self movement, tickling is perceived[1].

The rodent vibrissal system is advantageous for studying the mechanisms underlying sensorimotor integration during active sensation because movement and sensory input can be tracked with high precision[2–7]. Rodents explore the tactile world by moving their mystacial vibrissae (whiskers) rhythmically[2,3,6] in directed bouts of whisking lasting several whisking cycles (approximately 50 ms per cycle in mice)[6,8]. Whisking thus involves vibrissa movement over multiple time scales: the single whisking cycle and directed whisking bouts lasting hundreds of milliseconds.

Head-fixed mice can discriminate two object locations in the azimuthal plane, even with a single whisker[6]. Under these conditions, mice have to interpret whisker touch in the context of whisker movement to detect objects at particular locations[8,9]. Rodents solve this task by using a directed whisking strategy, favoring one of the two object locations[2,6,9]. At least two algorithms, which rely on distinct tactile cues, could underlie this form of object location discrimination. First, mice could extract object location as the whisker position at the moment of touch[10]. This strategy relies on a high-fidelity, cycle-by-cycle representation of whisker position and a millisecond-timescale (that is, much shorter than a single whisking cycle) coding of touch but does not require coding of the forces acting on the whisker. Second, mice could decode the patterns and amplitudes of touch-related forces, which depend on the location of the object[5,7]. This strategy relies on knowledge of the range and direction of whisking during a bout but does not make reference to instantaneous whisker position and may not require millisecond-timescale precision in the coding of touch.

The vibrissal somatosensory cortex (vS1) is crucial for detecting an object at a particular location[6,11]. Contact between whisker and object evokes phasic spikes in all layers of the vS1 (refs. 12,13). Anatomical connections between sensory and motor areas allow for interactions between whisking and touch[14]. Furthermore, the vS1 is the target of efferent signals from the motor cortex[15,16], which controls task-related whisking[17], and reafference signals, which arise in sensory neurons and ascend through multiple thalamic nuclei into the cortex[18,19]. Whisker position is represented at the level of spikes and membrane potential in the vS1 (refs. 20,21). These observations suggest that signals associated with whisking and touch interact in the vS1.

Here we probe how touch is interpreted in the context of whisker movement during a task in which mice discriminate two object locations (also referred to as 'object localization' in some previous studies[2,6,8]) using a single whisker. We focus on layer 4 (L4) neurons in the vS1. L4 neurons in individual barrels (approximately 2,000 neurons per barrel) process information from single whiskers[22–24]. L4 stellate cells receive the majority of the excitatory input from the sensory thalamus and additional input from other L4 stellate cells[22,25,26]. They project to L2/3 and L5 in the barrel cortex[22]. Barrels in L4 of the vS1 thus form a bottleneck, linking information related to sensation with a particular whisker and cortical processing.

[1]Janelia Farm Research Campus, Howard Hughes Medical Institute, Ashburn, Virginia, USA. [2]Present addresses: The Solomon H. Snyder Department of Neuroscience and Brain Science Institute, Johns Hopkins University School of Medicine, Baltimore, Maryland, USA (D.H.O.), Department of Zoology and Physiology, University of Wyoming, Laramie, Wyoming, USA (Q.-Q.S.) and Department of Basic Neurosciences, University of Geneva, Geneva, Switzerland (D.H.). [3]These authors contributed equally to this work. Correspondence should be addressed to K.S. (svobodak@janelia.hhmi.org).

Received 19 March; accepted 5 May; published online 2 June 2013; doi:10.1038/nn.3419

L4 neurons respond to whisker touch with short-latency spikes with timing jitter on the order of a few milliseconds[23,24]. When referenced to a neural representation of the rapidly changing whisker position or whisking phase[20,21], millisecond-timescale spike latency provides information about object location[14,27]. L4 neurons also encode the strength of the interaction between whisker and object, yielding alternative cues about object location.

We used behavioral analysis, electrophysiology and optogenetics to examine how whisker movement and touch can together discriminate object location. Mice solved the location discrimination task by preferentially whisking in one of two object locations, perhaps maximizing the difference in the number of touches and whisker forces between object locations[6,12]. One interpretation is that mice convert object location discrimination into detecting the object in one of the two locations[6]. To reveal the timescale of the integration of L4 spikes and whisker movements, we coupled channelrhodopsin-2 (ChR2) photostimulation[28,29] in L4 neurons to whisker position with millisecond precision. Mimicking touch-evoked activity in L4 neurons was sufficient to evoke behavior consistent with the illusory perception of an object in a target location but only in the C2 representation area of the vS1. Temporally precise coupling between activity and whisker movement was not required for this illusion, but photostimulated activity had to occur coincident with bouts of directed whisking to evoke the illusory perception of touch with a target object. These results suggest a spike count code underlying object location discrimination within defined regions of the cortical space and defined behavioral epochs lasting for at least a full whisk cycle. Our experiments further illustrate the power of combining trained perceptual behaviors, neuronal recordings and closed-loop, cell type–specific optogenetic perturbations in dissecting neural coding in complex, hierarchical circuits.

RESULTS

Neuronal encoding of object location

We trained head-fixed mice to perform a memory-guided, whisker-based object location discrimination task with the C2 whisker (**Fig. 1a**,**b**)[6]. In each trial, we moved a pole into one of two locations arranged in the posterior-anterior direction on one side of the head. High-speed videography and automated whisker tracking allowed us to reconstruct whisker movements and detect contacts between whisker and pole with millisecond precision[4,6]. Mice reported their decision about object location with licking or not licking. All experiments were performed in trained mice (n = 33 mice; fraction of trials correct, 0.75 ± 0.08 (mean ± s.d.); Online Methods).

Mice typically began to whisk before the pole came within reach and continued throughout the 'exploration window' (Online Methods; the epoch between the trial start cues and the typical response was 1.20 ± 0.16 s (mean ± s.d.)). Mice whisked with large amplitudes in short bouts (bout duration, 0.5–2 s; peak-to-peak amplitude, 44° ± 16° (mean ± s.d.); frequency, 17 Hz). Over the timecourse of learning, mice adjusted their setpoint of whisking[15] during the exploration window to roughly align with one of the pole locations[6] (**Fig. 1c**,**d**), which is a general feature of the whisking strategies in these types of tasks[2,9,16,17,30]. The region in space traversed by the whisker, the azimuthal region of interest (θ_{ROI}), was thus approximately centered on this pole location (**Fig. 1c** and **Supplementary Fig. 1**). For most experiments, the θ_{ROI} corresponded to the posterior pole location. We refer to trials with the pole near the center of the θ_{ROI} as 'YES trials' (in which the correct response was 'yes') and trials with the other pole location as 'NO trials' (in which the correct response was 'no'). In individual YES trials, the whisker typically touched the pole multiple times (mean, 4.09 times), whereas contacts were less frequent on NO trials (mean, 1.15 times) (**Fig. 1e**).

On the basis of loose-seal, cell-attached recordings, which sample neurons independently of their activity patterns, we estimate that 78% of L4 neurons within and near the active barrel are modulated by touch[12]. We recorded additional L4 neurons in and around the C2 barrel (<250 µm from the C2 center) during object localization with a single whisker (cell attached, n = 10; silicon probe, n = 21). We tracked whisker positions and contacts with 1-ms precision (**Fig. 1d**). Neurons rapidly excited by touch had short latencies (threshold latency, 8.7 ± 3.0 ms (mean ± s.d.); n = 13) and small jitter across trials (5.2 ± 1.3 ms for the first spike) (**Fig. 2a**,**b**).

Object location discrimination in the azimuthal plane requires the integration of information about whisker position and whisker touch[8,9]. Two different types of behavioral strategies could underlie object location discrimination. First, mice could extract the position of the whisker at the time of contact (**Fig. 3a**). This is plausible

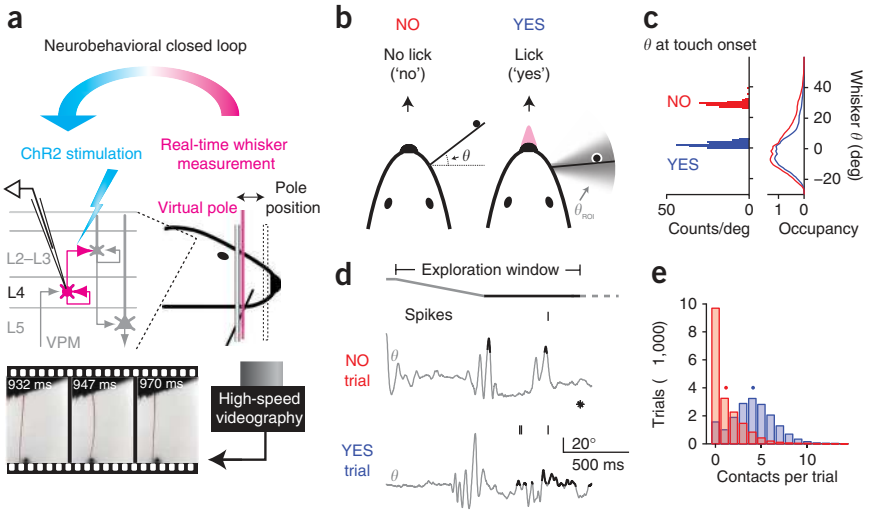

Figure 1 Overview of the experimental system and whisking strategy during object location discrimination. (**a**) Recordings were made from L4 neurons while mice localized objects with the C2 whisker. Whisker movements were measured with high-speed video. The mouse indicated its decision by licking for a water reward. Whiskers were detected as they crossed a virtual pole (infrared laser). A real-time system controlled photostimulation of ChR2-positive L4 neurons on the basis of whisker position. (**b**) Schematic of the object location discrimination task. θ is the azimuthal angle of the whisker at the base. Gray shading indicates the θ_{ROI}. (**c**) Whisking during object location discrimination (data from one representative session are shown). Left, whisker θ at touch onset (408 touches; YES trials, blue; NO trials, red). Right, distribution of whisker positions during task-related whisking (θ_{amp} > 2.5°). Occupancy (s) is the time spent at a particular θ (bin size, 1°). Deg, degree. (**d**) Whisker movements (gray, θ) in two example behavioral trials (top, NO trial; bottom, YES trial). The black trace segments correspond to contact periods. Pole entry (gray) and availability (black) are indicated in the top line. Protraction corresponds to increasing θ. Ticks, spikes; asterisk, lick. (**e**) The number of contacts per trial for all sessions (36,910 trials; YES trials, blue; NO trials, red). Dots, means.

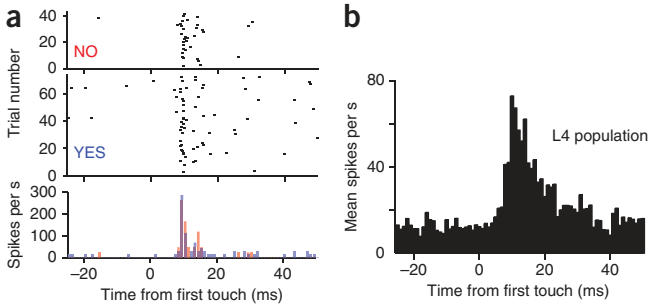

Figure 2 L4 neurons spike with precise latencies during object location discrimination. (**a**) Spike rasters and a peritouch spike histogram for one L4 neuron aligned to the first touch (same session as in **Fig. 1d**). (**b**) Peritouch spike histogram averaged across all rapidly touch-excited L4 neurons <250 μm from the C2 center (13 neurons) for the first touch per trial.

because the barrel cortex contains a neural representation of cycle-by-cycle whisker movement[20,21,27] and precisely timed contact signals (**Fig. 2a**,**b**). Second, the whisker interacts differentially with objects in different locations within the θ_{ROI} (for example, it reacts relatively strongly in the YES location). Object location within the θ_{ROI} can thus be derived by measuring contact forces without reference to rapid whisker movement. The directed whisking pattern adopted by mice in our task, in which θ_{ROI} was centered on one of the pole locations, was consistent with both strategies (**Figs. 1c–e** and **3a**).

These two behavioral strategies map onto distinct neural codes. Because of the small latency jitter (**Fig. 2a**,**b**), the spike-triggered position of the whisker (azimuthal angle, θ, at touch) differed for trials with different object locations (**Fig. 3b**). The timing of the synchronous activity in L4 referenced to rapid whisker movement[20,21,27] (spike timing) codes for whisker position at touch and thus for object location (**Fig. 3a**,**b**). However, because the whisker interacts more often, and probably more strongly[6], with the YES stimulus compared to the NO stimulus (**Figs. 1c–e** and **3a**), the number of spikes (spike count) also differed across object locations (**Fig. 3c**).

We compared the ability of these two neural codes to discriminate object location and behavioral choice by applying a linear classifier to each L4 neuron ($n = 31$). Across the population, object location was discriminated equally well using information about spike timing and spike count (**Fig. 3d**). Similarly, the mouse's behavioral choice (yes or no) could be discriminated using both coding schemes, although spike count performed slightly better compared to spike-triggered θ ($P = 0.0085$) (**Fig. 3e**). To establish a causal link between these two aspects of L4 activity and perception, we independently manipulated the timing and rate of L4 activity using optogenetics.

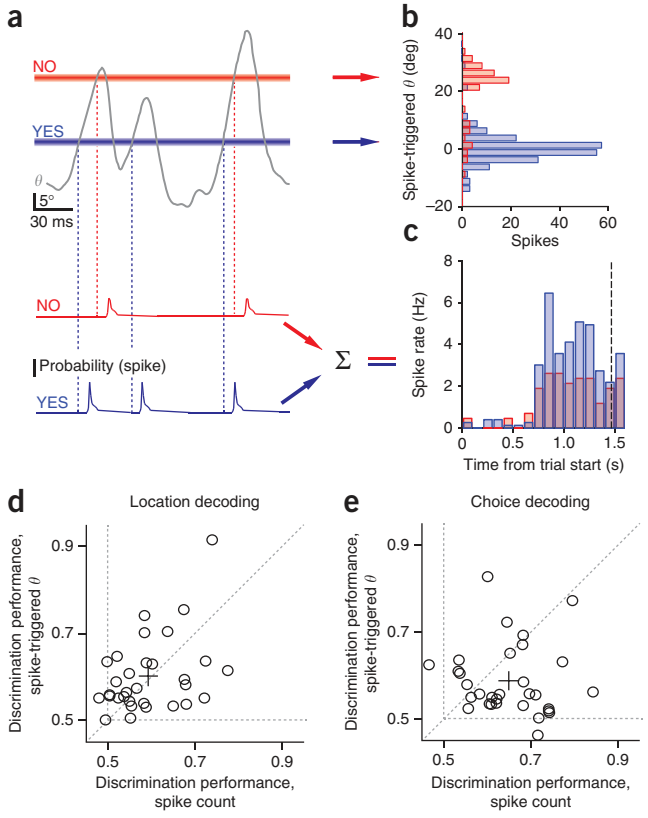

Figure 3 Decoding object location and behavioral choice on the basis of L4 spikes. (**a**) Neural coding of object location. Top, whisker position (θ, gray) and the two pole locations (blue, YES; red, NO). Bottom, schematic spike probability for the two object locations. (**b**) Spike-triggered θ (for every spike in the exploration window adjusted by the spike latency, 9 ms) (YES trials, blue, $n = 73$; NO trials, red, $n = 42$; same data as in **Fig. 2a**). (**c**) Spike count during the exploration window (same data as in **Fig. 2a**). Dashed line, mean reaction time. (**d**) L4 neurons discriminate object location equally on the basis of spike count and spike-triggered θ (circles, individual neurons; cross, population mean and standard error; $P = 0.57$ by paired two-tailed t test). Discrimination performance is the area under the receiver operating characteristic curve for a linear classifier. Dotted lines, chance discrimination performance and equal discrimination performance. (**e**) L4 neurons discriminate behavioral choice better on the basis of spike count than spike-triggered θ ($P = 0.0085$).

Closed-loop photostimulation of L4 causes illusory touch

Manipulations of activity during behavior can reveal the spike-train features that are decoded to drive decisions[31,32]. Manipulations in a closed loop with movement are necessary to establish causality between behavior and spike timing relative to movement. We thus developed methods to control activity in space and time, producing precise synthetic spike trains during behavior (**Figs. 1a** and **4a**).

To target L4 neurons in a specific barrel for photostimulation, we used transgenic mice expressing Cre recombinase selectively in their L4 neurons[25,33,34] together with an adeno-associated virus (AAV) expressing ChR2 (ref. 35) in a Cre-dependent manner[36]. We injected the virus into the C2 column guided by intrinsic signal imaging[37], resulting in ChR2 expression in L4 neurons in the vicinity of the C2 column (**Fig. 4a** and **Supplementary Fig. 2**).

We recorded light-evoked spikes from neurons in the C2 barrel column in awake mice using cell-attached recordings[12] (**Fig. 4b–d**). Brief light pulses (typically 1 ms; wavelength, 473 nm; intensity range, 5–32 mW mm^{-2}; Online Methods)[38] evoked spikes with short latencies (2.3 ± 1.2 ms (mean ± s.d.), $n = 12$), presumably directly triggered by light-gated current, in a subpopulation (50%, 12/24) of L4 neurons (**Fig. 4b–d**). We detected longer latency spikes in L2/3 (3.5 ± 1.1 ms, $n = 9$, $P < 0.05$ by one-tailed permutation test) and L5 (5.5 ± 4.0 ms, $n = 23$, $P < 0.01$ by one-tailed permutation test) cells, which is consistent with synaptic activation of these neurons[22] (**Fig. 4c**). Overall, single photostimuli and whisker contacts evoked similar activities across populations of L4 neurons (**Fig. 4e**).

We next asked whether photostimulating L4 neurons can evoke the illusory sensation of touch and perception of object location. We positioned a virtual pole, created by the beam of an infrared laser,

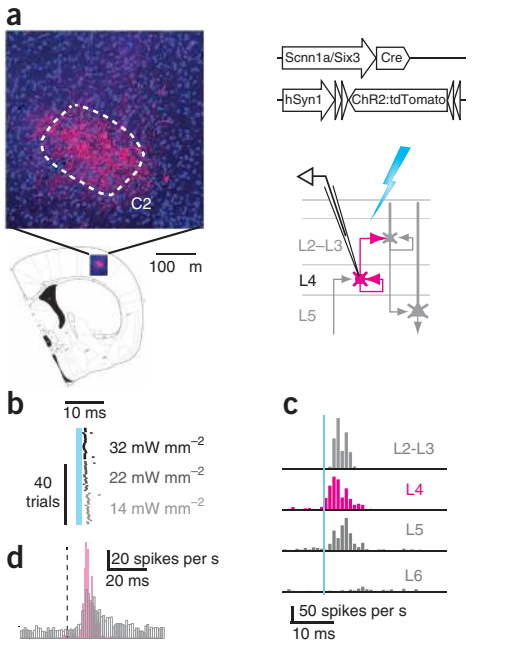

e

	Touch	Light
Neurons modulated by stimulus (%)	78	50
Spikes per stimulus (mean ± s.d.)	1.77 ± 0.77	1.03 ± 1.22
Latencies across cells (mean ± s.d., ms)	8.69 ± 3.01	2.3 ± 1.2
Latency jitter across cells (mean ± s.d., ms)	5.16 ± 1.32	0.58 ± 0.39
Duration of population activity (FWHM, ms)	7.72	4.73

Figure 4 Optogenetic stimulation mimics touch-evoked spiking in L4 neurons. (**a**) Targeting ChR2 to L4 neurons. Left, ChR2 expression (magenta) in one barrel (white dotted outline). Right, genetic scheme. (**b**) Single example of a neuron responding to different light intensities. Cyan, photostimulus. (**c**) Population peristimulus time histograms recorded in different cortical layers ($n = 85$ neurons total) after a ChR2 stimulus. Responses are averaged across light intensities (Online Methods). (**d**) Overlay of the population peristimulus time histograms (gray, touch; same data as in **Fig. 2b**; magenta, photostimulation, delayed by 5 ms from the stimulus). (**e**) Comparison of L4 activity evoked by touch and photostimulation.

next to one of the pole positions along the whisker (**Figs. 1a** and **5a**). A photodiode and real-time computer system detected the whisker crossing the virtual pole and also controlled the photostimulus with submillisecond precision. This temporal precision is necessary because mouse whiskers move with azimuthal speeds of up to 5° per millisecond[6]. The closed-loop system allowed us to mimic touch-evoked activity in L4 (duration of evoked population activity, full width at half maximum (FWHM) with photostimulation, 4.73 ms; with touch, 7.72 ms; **Fig. 4e**).

We performed all behavioral experiments on mice trained only on the object location discrimination task. In a subset of trials (25%), we delivered photostimuli coupled to whisker crossings (**Fig. 5a–c**). We used an equal probability of photostimulation in each trial type (YES or NO); pole location, but not photostimulation, predicted reward. A single light pulse (typically 1 ms, 41 mW mm^{-2}) was triggered per whisker crossing, producing approximately one action potential, which was similar to the activity evoked by single touches (**Fig. 4e** and **Supplementary Fig. 3**)[38]. Mice 'palpated' the virtual pole multiple times per trial, triggering a corresponding number of photostimuli (**Fig. 5b** and **Supplementary Fig. 4**). On the basis of the touch-to-spike latencies measured during the discrimination behavior (~9 ms; **Fig. 4d** and **Supplementary Figs. 3** and **4**), we chose 5 ms as the delay between whisker crossing and photostimulation. Similarly to actual contacts, whisker crossings were thus followed by synchronized activity in subpopulations of L4 neurons in the relevant barrel (total delay of whisker crossing to evoked spike, ~9 ms; **Fig. 4d,e**).

To determine whether photostimulation of L4 neurons is sufficient to evoke the illusory perception of object location, we focused our analysis on the NO trials, with the virtual pole centered in the θ_{ROI} and the actual pole toward the edge of the θ_{ROI} (**Fig. 5a**).

With photostimulation, mice were more likely to respond yes, consistent with photostimulation evoking a sensation of 'illusory touch' at the YES location. We used the difference in yes response probabilities between stimulated and nonstimulated NO trials to quantify illusory touch (fooling index, 0.21 ± 0.06 (mean ± s.d.); $n = 6$ mice; $P < 0.001$ by two-tailed t test) (**Fig. 5d,e**). Responses consistent with illusory touch in the YES location were evoked in about half of the stimulated NO trials starting in the first behavioral session with photostimulation ($P = 0.008$ by permutation test) (**Fig. 5e**). Laser light by itself, without triggering L4 activity, had no effect (fooling index, 0.002 ± 0.051;

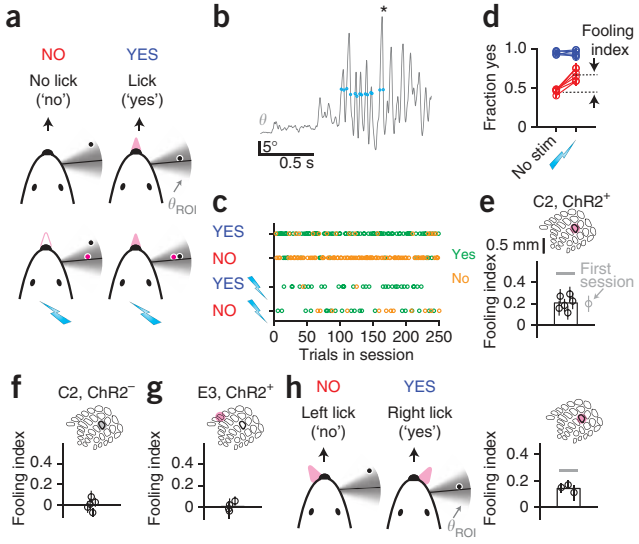

Figure 5 Closed-loop photostimulation causes illusory perception of object location. (**a**) Four trial types during a photostimulation behavior session depending on pole location and photostimulation (cyan lightning bolts). The virtual pole (magenta) was in the θ_{ROI}. Mice reported object location by licking or not licking. (**b**) Photostimulation (blue circles) coupled to whisker movement (gray, θ) during object location discrimination. Asterisk, answer lick. (**c**) Responses in the four trial types across one behavioral session. Green, yes responses; gold, no responses. (**d**) Photostimulation in NO trials (red) in the C2 barrel increases the fraction of yes responses. Blue, YES trials; stim, photostimulation. Error bars, s.e.m. Each line represents an individual mouse. (**e**) Fooling index (as defined in **d**). Black circles, individual mice; gray circle, first session averaged across all mice. Error bars, s.e.m. Gray bar, mean maximum possible fooling index. (**f**) Same experiment as in **a**–**e** but without ChR2 expression. Error bars, s.e.m. (**g**) Same experiment as in **a**–**e** but with ChR2 expression and photostimulation in the E3 barrel. Error bars, s.e.m. (**h**) Symmetric response task; both object locations were indicated by licking at one of two lickports (left or right lick). Black circles, individual mice. Gray bar, mean maximum possible fooling index. The performance of each mouse was different from zero as determined by one-tailed permutation test. Error bars, s.e.m.

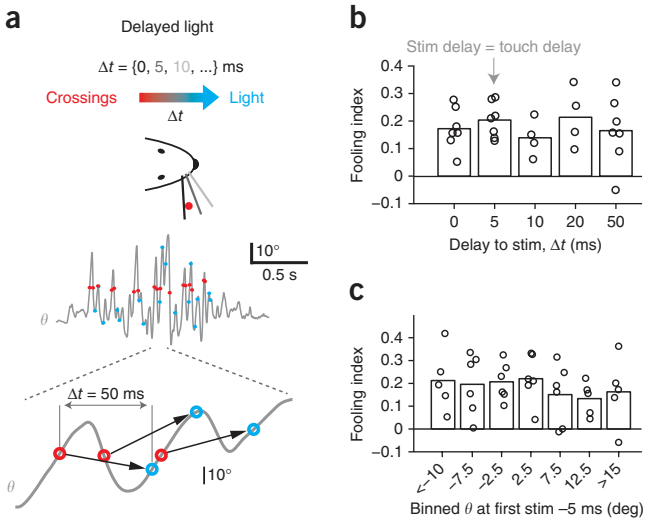

Figure 6 Precise millisecond-timescale spike latencies are not required for detecting an object at a particular location. (**a**) Top, delayed photostimulation of L4 neurons was triggered by whisker crossings with varying delays (Δt). Bottom, whisker movements with whisker crossings (red circles) and corresponding photostimuli (cyan circles) for Δt = 50 ms. (**b**) Fooling index as a function of the delay between whisker crossing and photostimulation. (**c**) Fooling index as a function of azimuthal angle at the time of stimulation.

$P = 0.93$; $n = 5$ mice) (**Fig. 5f**). Illusory touch was also evoked with the YES and NO locations reversed (with NO posterior and YES anterior; **Supplementary Fig. 5**).

We next performed experiments to determine whether mice read out L4 activity in general or only respond to activity in the somatotopic location corresponding to the spared whisker (C2). We introduced ChR2 into the E3 barrel 750 µm from C2. As before, we trained these mice to discriminate object locations with the C2 whisker. Stimulation of the E3 barrel did not produce illusory touch (fooling index, 0.004 ± 0.034; $P = 0.87$; $n = 4$ mice) (**Fig. 5g**). These experiments show that mice attend to cortical activity in a particular somatotopic location defined by perceptual learning and ignore activity in other locations. In addition, these experiments rule out nonspecific effects of light-evoked activity.

We next addressed the possibility that photostimulation of neurons in the attended somatotopic location could somehow trigger yes responses (licking) independently of perception of object location. We trained mice in a task in which both object locations were indicated by licking at one of two lickports ('symmetric response task'; **Fig. 5h**). Yes responses corresponded to licking to the right, and no responses corresponded to licking to the left. Under these conditions, mice again focused their whisking on one of the pole locations (**Fig. 5h** and **Supplementary Fig. 6**). The whisking strategy used by the mice is thus related to object location discrimination and is independent of how reward is coupled to the stimulus. As before, we introduced the virtual pole within the θ_{ROI} and analyzed the responses in NO trials. Mice were more likely to respond yes after photostimulation (**Fig. 5h**). These experiments show that precisely timed photostimulation in neuronal ensembles defined by infection with AAV virus and Cre expression can evoke illusory perception of object location. Moreover, a trial-by-trial analysis of behavioral responses, photostimulation and whisker-pole contact indicated that photostimulation and real touch showed similar patterns of behavioral saturation, partly occluded one another and were largely interchangeable (**Supplementary Fig. 7**).

Precisely timed spikes are not required

We tested whether illusory touch in the YES location required precise spike timing with respect to a whisker position signal representing cycle-by-cycle whisker movement. We varied the photostimulation latency (time between virtual pole crossing and photostimulation, Δt) over a range of 0–50 ms (**Fig. 6a**; 'delayed' light). At Δt = 0 ms, light-evoked spikes occur before touch-evoked activity would have occurred. At $\Delta t \geq 20$ ms, whisker position at the time of photostimulation spanned the entire θ_{ROI} (**Supplementary Fig. 8a**). This is because the retraction phase of whisking is extremely fast (<20 ms; **Fig. 6a**). There was no relationship between photostimulation latencies and fooling index (**Fig. 6b**; $P = 0.73$ by analysis of variance). This demonstrates that illusory touch in the YES location can be induced over a wide range of latencies corresponding to whisker positions throughout the θ_{ROI}.

In these experiments, we delayed all stimuli as a block, and the pattern of activity (that is, the sequence of interphotostimulation intervals) was thus preserved. In a separate set of experiments, we applied photostimulus trains that were statistically identical but did not correspond to the pattern of whisker crossings within a trial ('shuffled light' trials; the pattern of photostimuli matched the pattern of virtual pole crossings from five trials previous). Mice were still fooled, although the effect was smaller than in the standard experiment (**Supplementary Fig. 8b,c**; fooling index, 0.12 compared to 0.20 in the standard experiment; one of three mice, $P < 0.05$ by two-tailed permutation test). These experiments show that illusory touch does not require L4 activity to match the precise pattern of virtual pole crossings. We further examined whether illusory touch in the YES location varied with the position of the whisker at the time of the initial photostimulation. We did not detect position dependence (**Fig. 6c**; $P = 0.84$ by analysis of variance). Together these experiments indicate that perception of object location in our task does not depend on L4 activity being interpreted with reference to whisker position on a millisecond timescale.

Reducing spike count biases mice toward no responses

Our photostimulation experiments show that mice did not use spike latencies with respect to a cycle-by-cycle representation of whisker position for object location discrimination. We next tested whether spike count in excitatory neurons could explain the behavioral choices of the mice. We optogenetically stimulated GABAergic neurons of the C2 column using VGAT-ChR2 mice[39] (**Fig. 7a**) during the exploration window when mice whisked to sample the pole locations. Optogenetic inhibition reduced the touch-evoked activity of excitatory neurons to 57% of baseline ($P = 0.007$ by paired two-tailed t test; Online Methods). If mice rely on the precise spike latency to decide between yes and no responses, then optogenetically reducing spike count should not differentially affect performance in YES and NO trials. However, if mice base their decision on differences in spike count, then silencing should improve performance in NO trials but decrease performance in YES trials. Consistent with a spike count code, silencing in YES trials reduced performance (**Fig. 7b**; mean reduction in the fraction of trials correct, 0.43; all mice, $P < 0.001$ by one-tailed permutation test), and silencing in NO trials improved performance (**Fig. 7b**; mean increase in fraction trials correct, 0.24; all mice, $P < 0.01$).

To rule out the possibility that mice were simply confused or otherwise stopped licking after silencing, we performed the silencing experiment using the symmetric, lick left, lick right version of object location discrimination (**Fig. 5h**). Under these conditions,

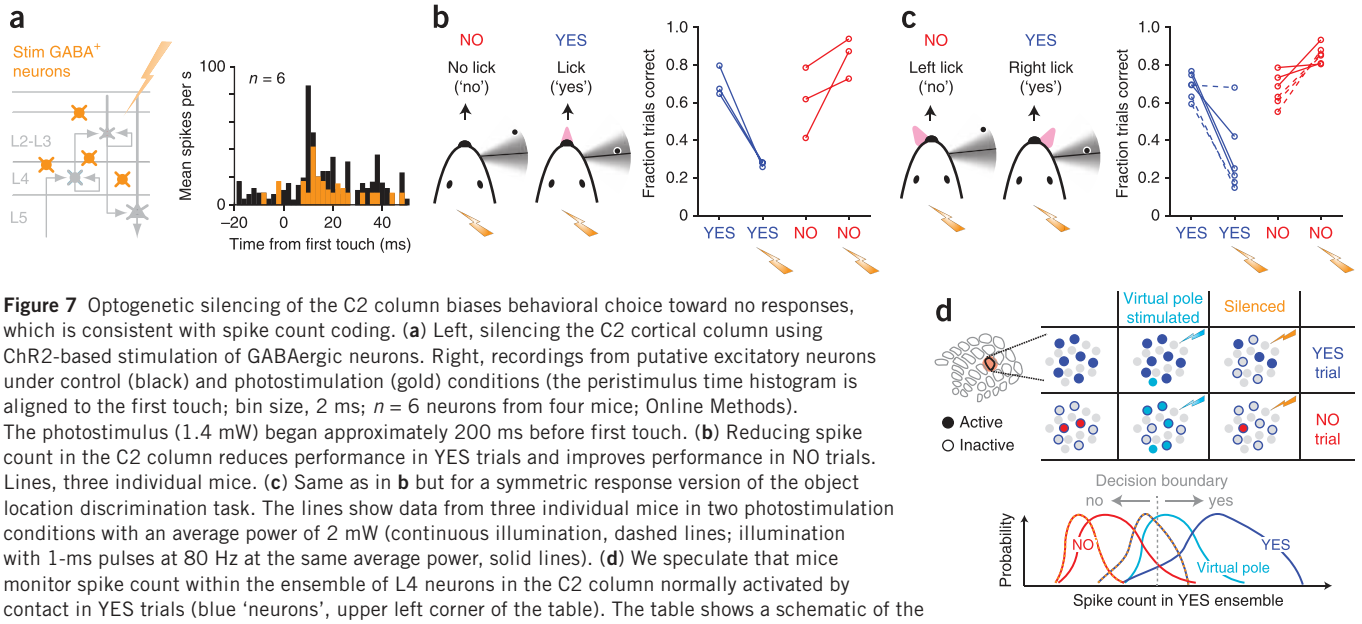

Figure 7 Optogenetic silencing of the C2 column biases behavioral choice toward no responses, which is consistent with spike count coding. (**a**) Left, silencing the C2 cortical column using ChR2-based stimulation of GABAergic neurons. Right, recordings from putative excitatory neurons under control (black) and photostimulation (gold) conditions (the peristimulus time histogram is aligned to the first touch; bin size, 2 ms; $n = 6$ neurons from four mice; Online Methods). The photostimulus (1.4 mW) began approximately 200 ms before first touch. (**b**) Reducing spike count in the C2 column reduces performance in YES trials and improves performance in NO trials. Lines, three individual mice. (**c**) Same as in **b** but for a symmetric response version of the object location discrimination task. The lines show data from three individual mice in two photostimulation conditions with an average power of 2 mW (continuous illumination, dashed lines; illumination with 1-ms pulses at 80 Hz at the same average power, solid lines). (**d**) We speculate that mice monitor spike count within the ensemble of L4 neurons in the C2 column normally activated by contact in YES trials (blue 'neurons', upper left corner of the table). The table shows a schematic of the L4 ensemble under the conditions tested in this study (**Figs. 5–7**). For example, in NO trials, a distinct but overlapping ensemble is activated (red neurons; the YES trial ensemble is indicated with blue outlines). In photostimulated NO (virtual pole, cyan) trials, activity is evoked in a subset of the YES ensemble, fooling mice into making yes responses. Bottom, hypothetical distribution of the decision variable (spike count in YES ensemble) used by mice to decide between a yes and a no response. Red, NO trials; blue, YES trials; cyan, NO trials with virtual pole and photostimulation (**Figs. 5** and **6**); gold dashed lines, silencing. If spike count in the YES ensemble of neurons exceeds a threshold value (the 'decision boundary'), the mouse makes a yes response; otherwise the mouse makes a no response.

performance in YES trials was also decreased (**Fig. 7c**; mean reduction in fraction trials correct, 0.37; all mice, $P < 0.001$), whereas performance in NO trials was increased (**Fig. 7c**; mean increase in fraction trials correct, 0.19; three mice, $P < 0.05$; one mouse, $P = 0.08$). Manipulating activity in the C2 column therefore shifts the balance between yes and no responses such that more activity among excitatory neurons was associated with more yes responses and less activity was associated with more no responses. Together our results suggest that mice measure spike count in an ensemble of L4 neurons to determine whether touch occurred in the YES pole location (high spike count) or the NO pole location (low spike count) (**Fig. 7d**).

Illusory perception occurs only during tactile exploration

A preliminary trial-by-trial analysis suggested that illusory object perception was produced only when photostimulation coincided with task-related bouts of whisking (**Supplementary Fig. 8c**). Because whisking often began shortly after the trial start cues (masking flash and the audible onset of pole movement) and continued through most of the exploration window, there were few trials in which photostimulation did not overlap with whisking. To improve our statistical power, we supplemented this data set with two additional experiments. We shifted the onset of the masking flash, which signaled trial start, earlier so that it preceded the pole motion by 1 s.

This prompted more variable onset of whisking in the exploration window with clear separation between bouts of whisking and rest periods (whisking $\theta_{amp} > 2.5$; **Fig. 8a**). To achieve photostimulation at variable times with respect to whisking bouts, we then photostimulated with either 20 pulses at 20 Hz (corresponding to the mean interphotostimulus interval in the experiments in **Figs. 5** and **6**; 0.053 ± 0.067 s (mean ± s.d.); $n = 68{,}552$ intervals) initiated 1 s before

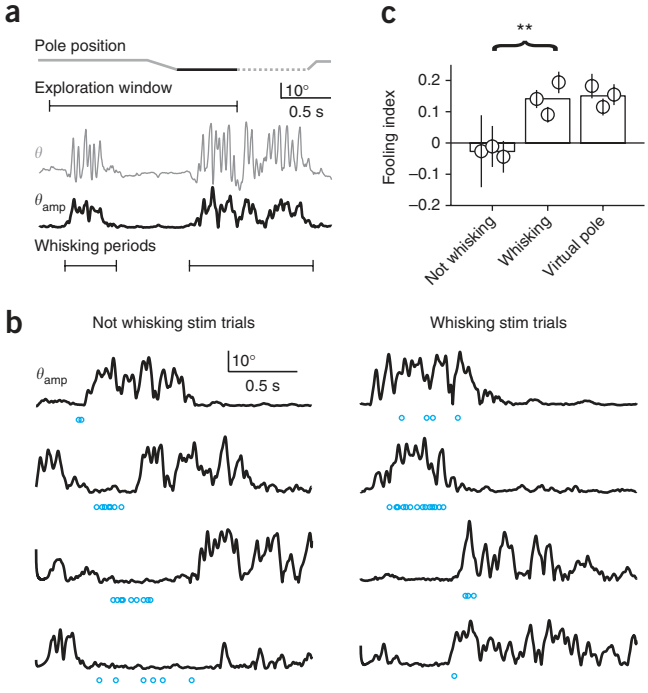

Figure 8 Illusory object location can be evoked only during periods of tactile exploration marked by whisking bouts. (**a**) Example of whisking bouts in relation to trial start and pole motion. Shown are whisker movement (θ, gray) and whisking amplitude (θ_{amp}, black). (**b**) Eight example trials showing the time course of whisking (θ_{amp}, black) and the corresponding photostimulation pattern (cyan circles). Left, trials in which photostimulation occurred during periods without whisking. Right, trials in which photostimulation occurred during whisking. (**c**) Fooling index for the whisking and not whisking trials. Also plotted are interleaved standard virtual pole trials ($\Delta t = 5$ ms, as in **Fig. 5e**). Error bars, s.e.m.

pole motion or pulses corresponding to the pattern of virtual pole crossings from five trials previous (the shuffled light trials; **Supplementary Fig. 8b**,**c**) but shifted 1 s earlier within the trial than when they would normally occur (Online Methods). We then pooled the trials of both types with the earlier shuffled light trials (**Supplementary Fig. 8b**,**c**). We sorted these pooled trials into 'not whisking' and 'whisking' categories on the basis of whisking amplitude during photostimulation (**Fig. 8b** and **Supplementary Fig. 8d**–**f**). During whisking bouts, the mice expressed robust illusory YES responses (**Fig. 8c**). If photostimulation coincided with rest periods, the mice showed no signs of illusory YES perception ($P = 0.001$ for whisking compared to not whisking trials pooled across mice, one-tailed permutation test). These experiments show that reports of perception of L4 activity are limited to bouts of tactile exploration in which active touch normally occurs (**Supplementary Fig. 9a**). In addition, L4 activity is ignored unless it is within the barrel corresponding to the moving whisker. Thus, perceptual reports of touch are gated by sensory expectation.

DISCUSSION

Patterns of action potentials propagating through a hierarchy of neural circuits code for features of the world and our actions within it[14]. Making sense of such systems requires measurements of activity in defined circuit nodes to develop hypotheses about neural coding and targeted perturbations to establish causal links between neural activity, perception and behavior[31,40,41].

Our experiments rely on cell type–specific[42], temporally precise quantitative photostimulation[38] to establish causal relationships between features of spike trains and perceptual behavior. Closed-loop control further allowed us to couple behavior and precise stimuli during active somatosensation. This real-time linkage between behavior and activity perturbations is important because normal perceptual behaviors are active[2,6,9,14,43]: representations of the environment are constructed from internal models of sensor movement and sensation[1]. Our study builds on pioneering work that used electrical microstimulation in simple perceptual tasks (for example, motion direction discrimination or tactile frequency discrimination) to link activity in defined brain regions to perception in passively stimulated animals[31,40].

Here we report that photostimulating a subset of L4 neurons was sufficient to evoke robust illusory touch sensation and perception of object location without training on photostimulation (**Fig. 5**). This is remarkable because there is a 50% overlap in L4 neurons phasically activated by touch and those activated by light (**Fig. 4e**). Furthermore, photostimulation activated only a subset of somatosensory pathways, bypassing the paralemniscal pathway and the superior colliculus[44]. Differences between activity produced by photostimulation and touch might explain why photostimulation was rarely successful in fooling the mice completely (**Fig. 5c**,**e**).

During tactile behavior, L4 neuron spikes showed latency precision that could be used to discriminate object locations (**Fig. 3b**,**d**). Despite this, several lines of evidence show that mice determined pole position on the basis of spike count rather than spike latency. First, adding spikes by L4 photostimulation in NO trials increased the proportion of yes responses (**Fig. 5c**–**e** and **Supplementary Fig. 7**). Second, decoupling L4 activity from whisker position in time did not change the degree of fooling (**Fig. 6**). Third, spike count decoded the behavioral choice better than spike latency (**Fig. 3e**). Fourth, in NO trials, touches were associated with a higher error rate (yes responses) compared to in trials without touches (**Supplementary Fig. 7**), indicating that mice did not use precise knowledge of whisker position at the time of contact in deciding on a response. Fifth, reducing spike count systematically biased behavioral choice toward no responses (**Fig. 7**).

Mice solved our task by preferentially moving their whiskers in the vicinity on one of two object locations, perhaps attempting to maximize the spike count difference between object locations[6,12]. This feature of the whisking strategy was similar for different pole positions (**Fig. 1** and **Supplementary Fig. 5**) and reward contingencies (**Fig. 1** and **Supplementary Fig. 6**). The whisking strategy is analogous to searching for one of two light switches in a dark room, a problem that is typically solved by biased probing on the basis of remembered locations of the switches. One interpretation is that mice try to convert object location discrimination into a detection task (that is, detecting the pole in one of the two locations). The spike count code used by the mice might be coupled to the behavioral strategy.

However, a spike count code could more generally tell the animal about object location. Freely moving rodents rapidly scan their whiskers through a range of interest, similarly to the mice in our experiments. During natural behaviors, the position of the range of interest in space is continually adjusted by head movements and changes in whisking setpoint[45]. Forces exerted by objects onto whiskers will differ with object location relative to the range of interest, providing spike count clues about object location both in the azimuthal (**Supplementary Fig. 9**) and radial directions[5,7].

Precise spike timing might still have roles in the assessment of texture[46] or in interactions between multiple whiskers[47]. Furthermore, certain aspects of spike timing are probably required in our task. Synchronous activity of L4 neurons, evoked by touch or photostimulation (**Fig. 4c**), may be essential for driving appropriate downstream ensembles.

Numerous reports have documented stimuli selectively in vS1 neurons, including direction[23], velocity[48] and possibly even phase within the whisk cycle[27]. Future experiments using similar methods as those we introduced here could reveal the conditions under which these different aspects of tactile information are read out to inform behavior.

Photostimulation of L4 neurons evoked illusory touch only during epochs of tactile exploration defined by whisking and the expectation of informative touch (**Fig. 8**). We do not know whether activity evoked outside these epochs of exploration was not perceived or simply not acted upon, perhaps because the photostimulation-evoked sensation was unnatural or not interpretable as a result of a lack of appropriately coordinated sensory and motor activity patterns.

Multiple mechanisms probably collaborate in gating the stimulus-response chain between L4 activity and behavior. The vibrissal motor cortex sends signals coding for whisking amplitude to L1 of the vS1[16]. Pyramidal cells in the barrel cortex receive this input in their tuft branches in L1, whereas bottom-up sensory input, in part from L4 neurons, impinges mainly on the proximal basal dendrites[25]. L1 input increases neuronal gain and can promote dendritic calcium spikes and bursting with coincident input in the proximal basal dendrites[30,49]. The whisker position signal from the vibrissal motor cortex might selectively amplify activity related to touch during periods of tactile exploration. Similarly, cholinergic modulation and disinhibition might contribute in changing the gain of cortical networks during periods of attention[50].

Illusory touch could only be evoked in a specific somatotopic location corresponding to the trained whisker (**Fig. 5e**,**g**). During learning, the brain presumably learns to selectively read out activity in this area and ignore activity in other regions of the barrel cortex and other sensory areas. The underlying mechanisms are unclear but might include top-down modulation, such as spatially selective attention and barrel cortex plasticity associated with learning. Similar experiments to those

introduced here could be used to study fundamental mechanisms underlying spatial signal selection for optimal decision making.

METHODS

Methods and any associated references are available in the online version of the paper.

Note: Supplementary information is available in the online version of the paper.

ACKNOWLEDGMENTS

We thank M. Smear, M. Hooks, L. Petreanu, N. Sofroniew, A. Lee, H. Yang, D. Golomb and J. Dudman for comments on the manuscript, N. Sofroniew for valuable suggestions on experiments, S. Michael for histology, S. Sternson and L. Looger (Janelia Farm) for reagents, T. Harris, B. Barbarits, A. Leonardo, C. Culianu, V. Iyer and D. Gutnisky (Janelia Farm) for help with silicon probe recordings and M. Karlsson for help with spike clustering.

AUTHOR CONTRIBUTIONS

D.H.O., S.A.H., Z.V.G., N.L., J.Y. and Q.-Q.S. performed experiments. D.H., Z.V.G. and N.L. developed the symmetric response task paradigm. D.H.O., S.A.H. and K.S. planned the project. D.H.O., S.A.H., Z.V.G., N.L. and K.S. analyzed the data. D.H.O., S.A.H. and K.S. wrote the paper with comments from the other authors.

COMPETING FINANCIAL INTERESTS

The authors declare no competing financial interests.

1. Wolpert, D.M. & Flanagan, J.R. Motor prediction. *Curr. Biol.* **11**, R729–R732 (2001).
2. Knutsen, P.M., Pietr, M. & Ahissar, E. Haptic object localization in the vibrissal system: behavior and performance. *J. Neurosci.* **26**, 8451–8464 (2006).
3. Voigts, J., Sakmann, B. & Celikel, T. Unsupervised whisker tracking in unrestrained behaving animals. *J. Neurophysiol.* **100**, 504–515 (2008).
4. Clack, N.G. *et al.* Automated tracking of whiskers in videos of head fixed rodents. *PLOS Comput. Biol.* **8**, e1002591 (2012).
5. Pammer, L. *et al.* The mechanical variables underlying object localization along the axis of the whisker. *J. Neurosci.* **33**, 6726–6741 (2013).
6. O'Connor, D.H. *et al.* Vibrissa-based object localization in head-fixed mice. *J. Neurosci.* **30**, 1947–1967 (2010).
7. Bagdasarian, K. *et al.* Pre-neuronal morphological processing of object location by individual whiskers. *Nat. Neurosci.* **16**, 622–631 (2013).
8. Kleinfeld, D. & Deschenes, M. Neuronal basis for object location in the vibrissa scanning sensorimotor system. *Neuron* **72**, 455–468 (2011).
9. Mehta, S.B., Whitmer, D., Figueroa, R., Williams, B.A. & Kleinfeld, D. Active spatial perception in the vibrissa scanning sensorimotor system. *PLoS Biol.* **5**, e15 (2007).
10. Knutsen, P.M. & Ahissar, E. Orthogonal coding of object location. *Trends Neurosci.* **32**, 101–109 (2009).
11. Hutson, K.A. & Masterton, R.B. The sensory contribution of a single vibrissa's cortical barrel. *J. Neurophysiol.* **56**, 1196–1223 (1986).
12. O'Connor, D.H., Peron, S.P., Huber, D. & Svoboda, K. Neural activity in barrel cortex underlying vibrissa-based object localization in mice. *Neuron* **67**, 1048–1061 (2010).
13. de Kock, C.P., Bruno, R.M., Spors, H. & Sakmann, B. Layer- and cell-type–specific suprathreshold stimulus representation in rat primary somatosensory cortex. *J. Physiol.* (*Lond.*) **581**, 139–154 (2007).
14. Diamond, M.E., von Heimendahl, M., Knutsen, P.M., Kleinfeld, D. & Ahissar, E. 'Where' and 'what' in the whisker sensorimotor system. *Nat. Rev. Neurosci.* **9**, 601–612 (2008).
15. Hill, D.N., Curtis, J.C., Moore, J.D. & Kleinfeld, D. Primary motor cortex reports efferent control of vibrissa motion on multiple timescales. *Neuron* **72**, 344–356 (2011).
16. Petreanu, L. *et al.* Activity in motor-sensory projections reveals distributed coding in somatosensation. *Nature* **489**, 299–303 (2012).
17. Huber, D. *et al.* Multiple dynamic representations in the motor cortex during sensorimotor learning. *Nature* **484**, 473–478 (2012).
18. Poulet, J.F., Fernandez, L.M., Crochet, S. & Petersen, C.C. Thalamic control of cortical states. *Nat. Neurosci.* **15**, 370–372 (2012).
19. Yu, C., Derdikman, D., Haidarliu, S. & Ahissar, E. Parallel thalamic pathways for whisking and touch signals in the rat. *PLoS Biol.* **4**, e124 (2006).
20. Fee, M.S., Mitra, P.P. & Kleinfeld, D. Central versus peripheral determinants of patterned spike activity in rat vibrissa cortex during whisking. *J. Neurophysiol.* **78**, 1144–1149 (1997).
21. Crochet, S. & Petersen, C.C. Correlating whisker behavior with membrane potential in barrel cortex of awake mice. *Nat. Neurosci.* **9**, 608–610 (2006).
22. Lefort, S., Tomm, C., Floyd Sarria, J.C. & Petersen, C.C. The excitatory neuronal network of the C2 barrel column in mouse primary somatosensory cortex. *Neuron* **61**, 301–316 (2009).
23. Simons, D.J. Temporal and spatial integration in the rat SI vibrissa cortex. *J. Neurophysiol.* **54**, 615–635 (1985).
24. Armstrong-James, M., Fox, K. & Das-Gupta, A. Flow of excitation within rat barrel cortex on striking a single vibrissa. *J. Neurophysiol.* **68**, 1345–1358 (1992).
25. Petreanu, L., Mao, T., Sternson, S.M. & Svoboda, K. The subcellular organization of neocortical excitatory connections. *Nature* **457**, 1142–1145 (2009).
26. Lu, S.M. & Lin, R.C.S. Thalamic afferents of the rat barrel cortex: a light- and electron-microscopic study using *Phaseolus vulgaris* leucoagglutinin as an anterograde tracer. *Somatosens. Mot. Res.* **10**, 1–16 (1993).
27. Curtis, J.C. & Kleinfeld, D. Phase-to-rate transformations encode touch in cortical neurons of a scanning sensorimotor system. *Nat. Neurosci.* **12**, 492–501 (2009).
28. Boyden, E.S., Zhang, F., Bamberg, E., Nagel, G. & Deisseroth, K. Millisecond-timescale, genetically targeted optical control of neural activity. *Nat. Neurosci.* **8**, 1263–1268 (2005).
29. Li, X. *et al.* Fast noninvasive activation and inhibition of neural and network activity by vertebrate rhodopsin and green algae channelrhodopsin. *Proc. Natl. Acad. Sci. USA* **102**, 17816–17821 (2005).
30. Xu, N.L. *et al.* Nonlinear dendritic integration of sensory and motor input during an active sensing task. *Nature* **492**, 247–251 (2012).
31. Romo, R., Hernandez, A., Zainos, A., Brody, C.D. & Lemus, L. Sensing without touching: psychophysical performance based on cortical microstimulation. *Neuron* **26**, 273–278 (2000).
32. Histed, M.H., Ni, A.M. & Maunsell, J.H. Insights into cortical mechanisms of behavior from microstimulation experiments. *Prog. Neurobiol.* **103**, 115–130 (2013).
33. Madisen, L. *et al.* A robust and high-throughput Cre reporting and characterization system for the whole mouse brain. *Nat. Neurosci.* **13**, 133–140 (2010).
34. Liao, G.Y. & Xu, B. Cre recombinase-mediated gene deletion in layer 4 of murine sensory cortical areas. *Genesis* **46**, 289–293 (2008).
35. Nagel, G. *et al.* Channelrhodopsin-2, a directly light-gated cation-selective membrane channel. *Proc. Natl. Acad. Sci. USA* **100**, 13940–13945 (2003).
36. Atasoy, D., Aponte, Y., Su, H.H. & Sternson, S.M.A. FLEX switch targets channelrhodopsin-2 to multiple cell types for imaging and long-range circuit mapping. *J. Neurosci.* **28**, 7025–7030 (2008).
37. Masino, S.A., Kwon, M.C., Dory, Y. & Frostig, R.D. Characterization of functional organization within rat barrel cortex using intrinsic signal optical imaging through a thinned skull. *Proc. Natl. Acad. Sci. USA* **90**, 9998–10002 (1993).
38. Huber, D. *et al.* Sparse optical microstimulation in barrel cortex drives learned behaviour in freely moving mice. *Nature* **451**, 61–64 (2008).
39. Zhao, S. *et al.* Cell type–specific channelrhodopsin-2 transgenic mice for optogenetic dissection of neural circuitry function. *Nat. Methods* **8**, 745–752 (2011).
40. Salzman, C.D., Britten, K.H. & Newsome, W.T. Cortical microstimulation influences perceptual judgements of motion direction. *Nature* **346**, 174–177 (1990).
41. O'Connor, D.H., Huber, D. & Svoboda, K. Reverse engineering the mouse brain. *Nature* **461**, 923–929 (2009).
42. Luo, L., Callaway, E.M. & Svoboda, K. Genetic dissection of neural circuits. *Neuron* **57**, 634–660 (2008).
43. Yarbus, A.L. *Eye Movements and Vision* (Plenum Press, 1967).
44. Veinante, P., Lavallee, P. & Deschenes, M. Corticothalamic projections from layer 5 of the vibrissal barrel cortex in the rat. *J. Comp. Neurol.* **424**, 197–204 (2000).
45. Mitchinson, B. *et al.* Active vibrissal sensing in rodents and marsupials. *Phil. Trans. R. Soc. Lond. B* **366**, 3037–3048 (2011).
46. Jadhav, S.P., Wolfe, J. & Feldman, D.E. Sparse temporal coding of elementary tactile features during active whisker sensation. *Nat. Neurosci.* **12**, 792–800 (2009).
47. Panzeri, S., Petersen, R.S., Schultz, S.R., Lebedev, M. & Diamond, M.E. The role of spike timing in the coding of stimulus location in rat somatosensory cortex. *Neuron* **29**, 769–777 (2001).
48. Pinto, D.J., Brumberg, J.C. & Simons, D.J. Circuit dynamics and coding strategies in rodent somatosensory cortex. *J. Neurophysiol.* **83**, 1158–1166 (2000).
49. Larkum, M.E., Senn, W. & Luscher, H.R. Top-down dendritic input increases the gain of layer 5 pyramidal neurons. *Cereb. Cortex* **14**, 1059–1070 (2004).
50. Letzkus, J.J. *et al.* A disinhibitory microcircuit for associative fear learning in the auditory cortex. *Nature* **480**, 331–335 (2011).

ONLINE METHODS

Mice. All procedures were in accordance with protocols approved by the Janelia Farm Research Campus Institutional Animal Care and Use Committee. We report *in vivo* data from a total of 48 mice: L4 neuronal recordings, 9 mice (C57BL/6) (**Figs. 2** and **3**); L4 photostimulation behavior experiments, 24 mice (10 Six3Cre[34] and 14 Scnn1a-Tg3-Cre[33]) (**Figs. 4**–**6** and **8**); silencing, 6 VGAT-ChR2 mice[39] (**Fig. 7**); electrophysiological calibration of the light stimulus, 4 VGAT-ChR2 mice (**Fig. 7**); *in vivo* electrophysiology to calibrate photostimulation, 2 Six3Cre mice (2 Six3Cre and 6 Scnn1-Tg3-Cre mice were used for both behavior and calibration) (**Fig. 4** and **Supplementary Fig. 3**); measurement of adaptation to photostimulation, 2 Ai32-x-Scnn1a-Tg3-Cre[51] mice (**Supplementary Fig. 4**); behavioral light-detection experiment (**Supplementary Fig. 7f**), 1 mouse (Tg(Etv1-Cre)GM225Gsat with a sham infection). Additional mice were used for brain slice experiments (**Supplementary Fig. 10**). Mice of the appropriate genotypes were assigned to experimental conditions arbitrarily without explicit randomization or experimenter blinding. However, for roughly half the mice given virus injections, the experimenter was *de facto* blind to expression level until after all experiments were completed.

Object location discrimination task and high-speed videography. We used three variations on a whisker-based object location discrimination task described previously[6,12] with the following modifications: all mice performed the task using only the C2 whisker; use of a thinner stimulus pole (0.500-mm diameter class ZZ gage pin, Vermont Gage), which reduced passive contact with the whisker by the pole; no air puff punishment; and water was not pumped out of the lickport (that is, the mouse did not compete with a peristaltic pump for water rewards), as we found that mice effectively consumed all water, and pooling was not a problem. In the first variation (**Figs. 1**–**3**, **5a**–**g**, **6**, **7b** and **8**), we used a go or no-go task with the go stimulus located more posterior than the no-go stimulus (close to the resting position of the whisker)[6]. In silicon probe recording sessions, the go position was randomly chosen in each trial from a range of four relatively posterior positions spanning 4.29 mm[17]. In the second variation (**Figs. 5h** and **7c** and **Supplementary Fig. 6**), we used a lick-left or lick-right task in which both stimulus locations were rewarded. The posterior pole position required a lick at the right-side spout, whereas the anterior pole location required a lick at the left-side spout. If the mouse first licked at the incorrect spout, the trial was scored as incorrect and a timeout punishment was given. Trials without responses were rare (fewer than 2% of trials in the experiment shown in **Fig. 5h**). Typical bias toward one of the two lickports is shown in **Figure 7c**. The third variation (**Supplementary Fig. 5**) was a go or no-go task in which the rewarded (go) stimulus location was more anterior and further from the resting position of the whisker than the no-go stimulus. This change in the reward contingency produced markedly different whisking (**Supplementary Fig. 5b**).

After mice achieved high performance with full whisker fields (typically >80% correct), their right whiskers were trimmed to C-row whiskers (the left side was left untrimmed). After performance stabilized in this condition, mice were trimmed to C2.

We used an optical 'lickport' to record licks and deliver water rewards for the go or no-go experiments[6]. We also used a two-spout electrical lickport[52] for the lick-left or lick-right task and for some go or no-go sessions (with one spout disabled). The pole locations were 11.6–15.25 mm from midline, and the anterior-posterior offset of the pole locations was 4.29–5.71 mm, corresponding to 23–30° of the azimuthal angle.

Video (1 kHz) was acquired for at least 2 s per trial starting before pole movement and ending after the response. Images were acquired with a Basler 504k camera and Streampix 3 software (Norpix) using a telecentric lens (Edmund Optics) and 940-nm illumination (Roithner Laser). Whisker tracking was performed with the Janelia Whisker Tracker (https://openwiki.janelia.org/wiki/display/MyersLab/Whisker+Tracking)[4,6]. Video frames with contact between whisker and pole were identified on the basis of the proximity between the whisker and pole and whisker curvature changes induced by the pole. In electrophysiology recordings, all contacts were further inspected manually. We report here the analysis of 147,269,000 frames of video from 70,756 behavioral trials during the ChR2 photostimulation experiment, plus an additional 13,896,000 frames of video from 3,088 behavioral trials from the L4 neuronal recording experiments.

Optogenetic targeting of cortical L4 neurons. We used two types of adult (older than postnatal day 60) male transgenic mice expressing Cre recombinase in L4 neurons (**Supplementary Fig. 10**). In Scnn1a-Tg3-Cre mice[33] (Jackson Labs: 009613, B6;C3-Tg(Scnn1a-cre)3Aibs/J), Cre expression is restricted to L4 stellate cells. Six3-Cre mice[25] were obtained by backcrossing Six3-Cre, line #69 for at least nine generations to C57BL/6Crl mice (Charles River). These mice express Cre in both L4 stellate cells and L4 GABAergic neurons[33,34]. We used both types of mice in parallel because Scnn1a-Tg3-Cre mice also express Cre in the thalamus, whereas Six3-Cre mice do not. However, histological analysis of the experimental mice did not reveal retrograde infection or ChR2 expression in thalamic relay cells. The behavioral results using these two types of mice were indistinguishable (**Supplementary Fig. 10**).

To restrict ChR2 expression to L4 neurons, we used an AAV (serotype 2/5; AAV2/5-hSyn1-FLEX-hChR2-tdTomato). hSyn1-FLEX-hChR2-tdTomato was obtained by subcloning a PCR fragment containing the 930-bp human codon optimized ChR2 (hChR2), fused in frame to tdTomato[53] (linker: GCCGCGGCC), into an AAV-hSyn1-FLEX parent vector (gift of L. Looger) at the Xba1 and Fse1 sites. The resulting plasmid (pAAV-hSyn1-FLEX-hChR2-tdTomato; Addgene 41015) contained the AAV inverted terminal repeats and a cassette with the human synapsin-1 promoter, a Cre-dependent[36] (double floxed and inverted) open reading frame for hChR2-tdTomato, a woodchuck hepatitis post-transcriptional regulatory element (WPRE) and an SV40 poly(A) sequence. The AAV2/5 virus was produced by the Janelia Farm Molecular Biology Shared Resource.

Mice were implanted with titanium headposts for head fixation[12]. Intrinsic signal imaging was performed through the skull[37] with a layer of cyanoacrylate adhesive (Krazy Glue) or Krazy Glue covered with clear nail polish (Electron Microscopy Sciences) to reduce glare. For anesthesia, we used chlorprothixene (0.007 mg intramuscularly, ~0.36 mg per kg body weight; Sigma C1671) and isoflurane (~0.5% in O_2).

After 1–13 d, we injected the virus into the C2 or E3 barrels through a thinned region of the skull under isoflurane anesthesia (1.5–2%). The injection system comprised a pulled glass pipette (~30-µm outer diameter, either broken to a sharp edge or broken and then beveled; Drummond Scientific, Wiretrol II) back filled with mineral oil. A fitted plunger was inserted into the pipette and slowly advanced to displace the contents using a hydraulic manipulator (Narashige, MO-10). We injected 10 nl at each of three depths: 600 µm, 500 µm and 400 µm.

For a subset of the 'sham infection' experiments (**Fig. 5f**; $n = 3$ mice), we used AAV2/1-CAG-FLEX-hM4D-2A-GFP (gift from S. Sternson) containing the CAG promoter, a Cre-dependent hM4D-2A-GFP sequence[54] and WPRE and SV40 poly(A) sequences. For the remaining sham infections, mice ($n = 2$) were injected with AAV2/5- hSyn1-FLEX-hChR2-tdTomato, but in these experiments ChR2-tdTomato was not expressed for unknown reasons.

Virus expression was for 43–129 d (90 ± 25 d (mean ± s.d.)) before the behavioral photostimulation session. The final behavioral photostimulation session occurred after 47–183 d (105 ± 33 d) of virus expression. After training, but before the first photostimulation session, we constructed a black dental acrylic (Lang Dental) 'well', leaving a ~2-mm diameter patch of skull over the C2 (or E3) column unobstructed.

After the experiments, mice were perfused transcardially with PBS followed by 4% paraformaldehyde and 0.1 M phosphate buffer. To recover the location of ChR2 expression within the barrel map, the cortex was flattened between two glass slides, sectioned at 100 µm and processed for cytochrome oxidase[12]. Images of ChR2-tdTomato fluorescence within the cytochrome oxidase–stained barrel map were acquired on a macroscope (Olympus MVX10). The area showing ChR2-tdTomato–labeled neurons was outlined manually (**Supplementary Fig. 2**). For confocal imaging (Zeiss LSM 510) (**Fig. 4a**), coronal sections were mounted on glass slides using Vectashield mounting medium with 42,6-diamidino-2-phenylindole[12].

Real-time control of cortical L4 neurons. Behavior and photostimulation were controlled by open-source software (http://brodylab.princeton.edu/bcontrol; Z. Mainen, C. Brody & C. Culianu)[6,12]. Analog outputs for controlling photostimuli and masking light flashes were from a PCI-6713 board (National Instruments). The virtual pole (diameter ~0.5 mm, determined by beam diameter and experimenter-chosen photodiode voltage thresholds) was a laser beam produced by a laser diode (Thorlabs, CPS808; wavelength, 808 nm). The position of the virtual

doi:10.1038/nn.3419

pole was adjusted daily to lie next to one of the pole locations along the whisker. We imaged the intersection between the virtual pole and the whisker onto a photodiode (Hamamatsu, S9219). The light scattered by the whisker moving though the virtual pole was detected by the photodiode, amplified (Stanford Research Systems, Model SR570) and processed using the real-time control system (hard real-time task period or worst-case timing jitter, 0.1667 ms). Two intensity thresholds were set for each session. As the whisker passed through the virtual pole, first the low and then the high threshold was exceeded. When the photodiode signal exceeded the higher threshold, the whisker was considered to have 'crossed' the virtual pole. A new crossing could not occur until the photodiode signal dropped below the lower threshold.

Light from a 473-nm laser (CL-473-150, Crystal Laser) was gated by an acousto-optical modulator (AOM; MTS110-A3-VIS, Quanta Tech; extinction ratio, 1:2,000) and a shutter (Vincent Associates) under control of the real-time Linux system. Light exiting the AOM was focused into a multimode optical fiber (62.5 μm; Thorlabs) and recollimated. Each day the beam was positioned over the C2 or E3 column. The beam diameter was ~1.5 mm (99% energy).

Laser pulses were delivered to the brain through the skull, which was occasionally thinned, a thin layer of Krazy Glue and a thin layer of nonpigmented dental acrylic (Lang Dental). Laser power at the surface of this preparation was set for a given session at either ~73 mW (pulse duration of 1 ms) or ~56 mW (pulse duration of 1.333 ms) (intensities ~32–41 mW mm^{-2}). For 6/34 sham (ChR2-negative) sessions, we increased the dose to ~57 mW and 2 ms.

A separate data acquisition computer running Ephus (ephus.org) acquired the photodiode signal and the AOM control signal and triggered individual frames of high-speed video (all on the same clock, triggered by a master trigger from the real-time Linux system). This allowed us to align high-speed video frames with virtual pole crossings and photostimulation pulses without compensation for computer clock drifts.

To minimize the possibility that mice would see and respond to light pulses *per se* (that is, independent of neuronal excitation), in every trial a 'masking flash' pulse train (20 pulses at 10 Hz, 1–2 ms per pulse) was delivered using a custom light-emitting diode (LED) driver and 470-nm LEDs (Luxeon Star) positioned near the eyes of the mouse. The masking flash began as the pole started moving into reach and continued through the end of the period in which optogenetic pulses could occur. For experiments in which optogenetic pulses occurred before the start of pole movement ('early' light pulses; **Fig. 8**), the masking flash began 1 s before pole motion, and 30 masking flash pulses were delivered instead of 20. Mice were unable to solve the object location discrimination task visually. Performance of highly trained mice dropped to chance levels after the C2 whisker was trimmed (lick left or lick right, $n = 2$; lick or no lick, $n = 3$; $P > 0.26$).

Optogenetic silencing of the barrel cortex. VGAT-ChR2 mice were surgically implanted with custom stainless steel or titanium headposts for head fixation, and the dorsal surface of the skull was covered in Krazy Glue followed by a layer of clear dental acrylic (Lang Dental), which was polished using acrypoints (Acrylic Polishing Kit HP Shank, Pearson Dental). A thin layer of clear nail polish (Electron Microscopy Sciences, 72180) was applied to reduce light glare. Silencing was done with a 473-nm laser light centered on C2 through the polished skull, producing silencing in a tissue volume with radius 1 mm and comprising all layers (Z.V.G., N.L., K.S., unpublished data).

For the lick or no-lick experiment (**Fig. 7b**), the photostimulus was a pulse train (5-ms square wave pulses; 50 Hz; average power, 4 mW; CL-473-150, Crystal Laser) delivered with masking flash (1–2 ms at 10 Hz) beginning at the onset of pole motion for a fixed duration of 3.75 s. Silencing trials were a randomly chosen 25% of all trials. Data are shown as the means of trials pooled over one to four sessions per mouse and show 24–44 silencing trials per session and 44–151 silencing trials total per mouse (**Fig. 7b**).

For the symmetric-response, lick-left or lick-right experiment (**Fig. 7c**), stimulation was at a mean power of ~2 mW delivered either continuously or using a train of 1-ms square wave pulses at 80 Hz. The photostimulus began at the onset of pole movement for a fixed duration of 1.5 s (ending after the response cue, described below). Silencing trials were a randomly chosen 25% of all trials, never back to back. In addition, the symmetric response silencing experiment differed from the earlier experiments reported here in the following details: at the beginning of the exploration window, the vertical pole moved quickly (0.2 s) into reach of the C2 whisker, whereupon the mouse whisked to make contact with the pole. The pole was present for 1 s; the exploration window terminated when the vertical pole moved (0.2 s) out of reach of the C2 whisker. During the exploration window, mice were trained to withhold their licking response. After the exploration window, an auditory 'response' cue (pure tone, 3.4 kHz, 0.1-s duration; DigiKey, 458-1088-ND) was issued, and mice initiated licking. Licking early during the trial was punished by a loud 'alarm' sound (siren buzzer, 0.05-s duration; RadioShack, 273-079) followed by a brief timeout (1–1.2 s). Continued licking triggered additional timeouts. The trial was allowed to resume once the timeout was complete, but these trials were excluded from the analyses. Data (**Fig. 7c**) are shown as the means of trials pooled over 3–6 (4.3 ± 1.2 (mean ± s.d.)) sessions and comprising 66 ± 17 (mean ± s.d.) silencing trials per photostimulation condition (continuous or pulse) per mouse.

***In vivo* electrophysiology.** Spikes during the object location discrimination task were recorded using either loose-seal cell-attached recordings[12] or silicon probe recordings. After a loose seal was achieved, the behavioral protocol was initiated for 5–15 trials. Cells that did not show task-modulated activity were discarded. Numbers reporting the fraction of touch-modulated neurons were derived from previous loose-seal recordings[12].

For silicon probe recordings, on the first day of recording, a 1-mm diameter crainiotomy was opened above the C2 column. The dura was retracted using fine forceps (Dumot #5SF). We used probes with 32 pads distributed across four shanks (Neuronexus Buzsaki32-A32 and Buzsaki32Lsp-A32). Before each recording, the tips of the probe were brushed with DiI. The mouse was briefly anesthetized (2–3 min, 1.5% isoflurane) to remove the cement and silicon cap. The mouse was then mounted in the behavioral and recording apparatus. The probe was positioned on the surface of the cortex and photographed. Two drops of 1.5% Type III-A agarose in cortex buffer were applied to the well. The probe was lowered (1–2 μm s^{-1}, pausing 60 s every 30–50 μm) into the brain normal to the pial surface. If any of the shanks began to bend or the cortex dimpled, the probe and agarose were removed, and the process was restarted. Mice were awake and calm during probe descent. Behavioral protocols were initiated after probe location was finalized. Each behavioral session time, including probe insertion and removal, lasted 1.5–2.5 h. After a recording session, the well was filled with Kwik-Cast (WPI) and sealed with dental cement. On subsequent days (2–6 total days per mouse), the electrode was positioned >100 μm from the previous recording sites.

After the experiment, brains were fixed, and the brain was blocked at ~30° from the horizontal. The brain was lightly compressed between two glass slides, which flattened the barrel field. Slices were cut tangential to the cortical surface (100-μm thickness) and stained for cytochrome oxidase. DiI spots and surface photography were used to map recording day to location in the barrel map. Recording location was defined by triangulating the position of the center of each DiI spot to the three nearest barrels and then warping these points to a standard barrel map[55]. Putative L4 recordings were limited to sessions in which the manipulator depth from the surface minus the distance from tip to pad with maximum spike energy was 418–588 μm and the DiI spot terminated in either the slice containing the cytochrome oxidase staining or the next deeper slice.

Silicon probe voltage traces were digitized at 19,531.25 Hz and stored using a custom headstage (B. Barbarits & T. Harris, http://www.janelia.org/lab/apig-harris-lab) and custom software (C. Culianu & A. Leonardo). Raw voltage traces were bandpass filtered between 300 and 6,000 Hz (MATLAB 'idealfilter'). Common source noise was removed by sorting all 32 traces by amplitude for each time point and then subtracting the mean voltage of the middle 50% of sorted traces from each unsorted trace. Spikes were detected independently for each channel as threshold crossings above 4 s.d. of the channel. Events whose peak amplitudes across channels on the same shank occurred with <307.5 μs jitter were merged. For each event, waveforms for all eight channels on the shank were extracted and upsampled twice. Principal components analysis was performed on individual channels for all waveforms in the recording session that exceeded 4 s.d.

Putative single units were sorted by manual cutting in MatClust[56]. Each shank was sorted separately. The sorting parameters were spike amplitude, width and the first two principal components for all eight channels plus time (33 total parameters). After sorting, quality metrics were calculated[57]. Estimated false negatives from undetected spikes below the voltage threshold were <0.1% for all units. Estimated false negatives from censored-period exclusion ranged from 1.6% to 4.7%, mean 3.6% ± 1.0% (s.d.). Estimated false positives from interspike

interval violations between the censored and absolute refractory period ranged from 0% to 12.8% mean 1.2% ± 3.0% (s.d.), assuming a 10-Hz, independent, Poisson-spiking contaminating unit. A total of 148 units were sorted (mean of 7 per recording), of which 21 met the distance (<250 µm from the C2 center) and depth (see above) criteria to be considered near-C2, L4 units.

A comparison of the cell-attached to the silicon probe data set showed no significant differences in touch latency (mean, 8.6 ms compared to 9.0 ms (cell attached compared to silicon probe)), jitter (mean, 4.8 ms compared to 5.9 ms), decoding of behavioral choice (mean area under the curve (AUC) for spike count, 0.675 compared to 0.650; for spike-triggered θ, 0.610 compared to 0.587), spike count decoding of pole location (0.626 compared to 0.593) or evoked spikes per first contact (mean, 1.00 compared to 1.55). Cell-attached units had lower baseline firing rates (mean, 5.1 Hz compared to 13.2 Hz) and significantly better spike-triggered decoding of pole position (0.658 compared to 0.602; $P = 0.012$). These data suggest that silicon probe recordings may have a sampling bias for a functionally similar but more active set of L4 neurons than cell-attached recordings.

To calibrate the photostimulation pulses, we performed loose-seal cell-attached recordings in awake mice in the behavior apparatus[12] with the following modifications: (i) we covered the recording well and craniotomy with 4-(2-hydroxyethyl)-1-piperazineethanesulfonic acid–buffered artificial cerebrospinal fluid rather than a thick layer of agarose; and (ii) the craniotomy was larger (up to 1.5 mm in diameter). Eight of ten mice were the same as those used for the behavior experiments; the remaining two mice were prepared identically. Pulses occurred every 20 s. For each neuron, we stepped sequentially through pulses comprising 100%, 66%, 40% and (in most cases) 20% of maximum power, with a mean of 29 sweeps per neuron. The latency and number of evoked spikes were relatively weak functions of the applied light intensity in L4 (**Fig. 4b** and **Supplementary Fig. 3**). The maximum power was matched to that in our behavioral experiments (53 ± 3.6 mW (mean ± s.d.), range 45–57 mW, $n = 85$ neurons). Pulse duration was adjusted to roughly standardize the maximal light dose (1.38 ± 0.09 ms, range 1.333–1.667 ms). Because of the trade off between maximum intensity and pulse duration, to pool neurons we occasionally report 'relative power' as a percentage of the maximum power (**Supplementary Fig. 3e**,**f**).

To determine the reliability of L4 photostimulation-evoked responses during trains matching the whisking pattern, we recorded from ChR2$^+$ cells in loose-seal mode while replaying photostimulation trains corresponding to the whisking patterns in other experiments. For these recordings (**Supplementary Fig. 4**), we used mice derived from a cross between Scnn1a-Tg3-Cre and AI32 (a ChR2 Cre reporter[51]) mice. For each cell, 20 different trains of 1-ms pulses were delivered at a light intensity of two to three times the minimal power required to evoke a spike (range 0.85–2.5 mW; **Supplementary Fig. 4**). Spike latencies for each cell showed very low variability (0.59 ms s.d.) and were only weakly dependent on the interstimulus interval (**Supplementary Fig. 4b**). The probability of a spike being evoked by photostimulation was dependent on the interstimulus interval, with short intervals correlating to a reduced spike probability (**Supplementary Fig. 4c**). However, short interstimulus intervals were relatively rare, and the spike probability was on average a flat function of the sequential photostimulus number (first, second and so on; **Supplementary Fig. 4d**).

To characterize inhibition by photostimulation of GABAergic neurons in VGAT-ChR2 mice (**Fig. 7a**), we made silicon probe recordings near the C2 barrel column while mice performed the lick-left or lick-right task. Single units were sorted manually offline. We characterized cells with broad action potentials that were not excited by photostimulation. These are putative excitatory neurons. We further selected neurons that were rapidly excited by touch (5–25-ms time window) with 10–20 photostimulus trials (25% of all trials).

Data analyses. The exploration window comprised the period from the start cues (the start of pole movement and/or masking flash) until the answer lick response or 1.5 s later (capturing ~99% of reaction times), whichever came earlier. For presentation in the figures, traces of the whisker base angle, θ, were smoothed with a 5-ms moving average.

For decoding analyses (**Fig. 3**), we computed the area under the receiver-operating characteristic curve (MATLAB 'perfcurve') using as the decision variable either (i) the total spike count within the exploration window, n_s, or (ii) the mean spike-triggered θ, θ_s. Each neuron was considered independently. We assumed for decoding that the correct 'sign' (that is, the class giving higher decision-variable values) was known. That is, in predicting the class (object location or yes or no choice) for a given trial on the basis of the value of the decision variable, we treated higher decision-variable values as predicting the class that had the higher mean decision-variable value. Thus, values of AUC less than chance level (AUC = 0.5) could only occur for nondiscriminative neurons. We included trials both with and without contact.

For the analysis of fooling index (FI) compared to whisker angle at stimulation (**Fig. 6c**), we computed FI_i as

$$FI_i = \text{yes}_{\text{stim},i} - \text{yes}_{\text{ns}}$$

where $\text{yes}_{\text{stim},\,i}$ is the fraction of yes responses in trials where θ 5 ms before the time of the first light pulse was in the ith bin, and yes_{ns} is the overall fraction of yes responses in unstimulated NO trials within the session.

Whisking amplitude (θ_{amp}) was defined as the magnitude of the Hilbert transform of bandpass (6–60 Hz, Butterworth)-filtered θ[17]. For the 'shuffled' light experiments (**Supplementary Fig. 8b**,**c**), we chose a delay of five trials (N-5). Five trials was sufficiently short to ensure that the behavioral state (satiety, kinematics of whisking and so on) of the mouse was constant and sufficiently long to avoid occasional response dependencies over 1–2 trials (for example, impulsive licking). For the analysis of the whisking dependence of illusory object perception (**Fig. 8**), we considered light stimuli to occur during whisking when the mean θ_{amp} at the time of the light pulses was greater than 2.5° counting only light pulses occurring before the end of the exploration window. We pooled trials from the shuffled experiments described in **Supplementary Figure 8b**,**c**, as well as from new experiments in which light pulses were moved 1 s earlier in time ('early' light pulses). These early light sessions were either (i) shuffled light sessions in that the light pulses in trial N were taken from crossings in trial N-5 and then moved 1 s earlier or (ii) regular light sessions in which a train of 20 pulses at 20 Hz (1–1.333-ms pulse duration) was delivered 1 s before the start of the pole movement (that is, 1 s before the earliest time pulses could arrive during the basic experiment shown in **Fig. 5**).

Error bar s.e.m. values were calculated using bootstrap methods. We did not predetermine sample size using power analysis.

51. Madisen, L. *et al.* A toolbox of Cre-dependent optogenetic transgenic mice for light-induced activation and silencing. *Nat. Neurosci.* **15**, 793–802 (2012).
52. Slotnick, B. A simple 2-transistor touch or lick detector circuit. *J. Exp. Anal. Behav.* **91**, 253–255 (2009).
53. Shaner, N.C. *et al.* Improved monomeric red, orange and yellow fluorescent proteins derived from *Discosoma* sp. red fluorescent protein. *Nat. Biotechnol.* **22**, 1567–1572 (2004).
54. Armbruster, B.N., Li, X., Pausch, M.H., Herlitze, S. & Roth, B.L. Evolving the lock to fit the key to create a family of G protein–coupled receptors potently activated by an inert ligand. *Proc. Natl. Acad. Sci. USA* **104**, 5163–5168 (2007).
55. Maier, D.L. *et al.* Disrupted cortical map and absence of cortical barrels in growth-associated protein (GAP)-43 knockout mice. *Proc. Natl. Acad. Sci. USA* **96**, 9397–9402 (1999).
56. Karlsson, M.P. & Frank, L.M. Network dynamics underlying the formation of sparse, informative representations in the hippocampus. *J. Neurosci.* **28**, 14271–14281 (2008).
57. Hill, D.N., Mehta, S.B. & Kleinfeld, D. Quality metrics to accompany spike sorting of extracellular signals. *J. Neurosci.* **31**, 8699–8705 (2011).

doi:10.1038/nn.3419